3D environment modulates persistent lamin distribution and the biomechanical signature of the nucleus.

Raquel González-Novo[1], Héctor Zamora-Carreras[2], Ana de Lope-Planelles[1], Horacio López-Menéndez[3,4], Pedro Roda-Navarro[2], Francisco Monroy[3,4], Lin Wang[5], Christopher P. Toseland[6], and Javier Redondo Muñoz[1,*]

[1]Department of Molecular Biomedicine, Centro de Investigaciones Biológicas Margarita Salas, Madrid, Spain.

[2]Department of Immunology, School of Medicine, University Complutense de Madrid and 12 de Octubre Health Research Institute (imas12) Madrid, Spain.

[3]Department of Physical Chemistry, Complutense University, Madrid, Spain.

[4]Translational Biophysics, Hospital Doce de Octubre Health Research Institute (imas12), Madrid, Spain.

[5]Central Laser Facility, Research Complex at Harwell, Science and Technology Facilities Council, Rutherford Appleton Laboratory, Harwell, Oxford, UK.

[6]Department of Oncology and Metabolism, University of Sheffield, Sheffield, UK.

* To whom correspondence should be addressed. Tel: +348373112; Fax: +34915360432 Email: Javier.redondo@cib.csic.es

ABSTRACT

The interplay between cells and their surrounding microenvironment drives multiple cellular functions, including migration, proliferation, and cell fate transitions. The nucleus is a mechanosensitive organelle that adapts external mechanical and biochemical signals provided by the environment into nuclear changes with functional consequences for cell biology. However, the morphological and functional changes of the nucleus induced by 3D extracellular signals remain unclear. Here, we demonstrated that cells derived from 3D conditions show an aberrant nuclear morphology and mislocalization of lamin B1 from the nuclear periphery. We found that actin polymerization and protein kinase C (PKC) activity mediate the abnormal distribution of lamin B1 in 3D conditions-derived cells. Further experiments indicated that these cells show altered chromatin compaction, gene transcription and cellular functions such as cell viability and migration. By combining biomechanical techniques, such as force compression and single-nucleus analysis by atomic force microscopy, optical tweezers, and super-resolution microscopy, we have determined that the nucleus from 3D conditions-derived cells show a different mechanical behaviour and biophysical signature than the nucleus from control cells. Together, our work substantiates novel insights into how the extracellular environment alters the cell biology by promoting consistent changes in the chromatin, morphology, lamin B1 distribution, and the mechanical response of the nucleus.

INTRODUCTION

The cell nucleus is organized into the nuclear envelope and the underlying lamina network, which encloses the chromatin and controls multiple DNA functions (1). In the physiological context, cells have to respond to external stimuli, including biochemical signals, but also biomechanical properties of the extracellular microenvironment (3, 4). The mechanical response of the nucleus is dictated by the chromatin and the lamina network (5), which, in turn, is critical in multiple processes, including altered gene expression, cell fate transitions, cell migration, cell cycle progression, and tumorigenesis (6, 7).

Multiple biophysical techniques have been used to characterize the nuclear mechanics changes induced by multiple biomechanical techniques, such as cell stretching, substrate patterning, external compression, and 3D cell migration (8-10). Interestingly, studying the behavior of the nucleus in intact cells might lead to misinterpretation due to the cell membrane and the cytoskeleton; thereby, an integral study of intact cells and isolated nuclei might bypass this issue to better define the biophysical changes interpreted by the nucleus (11). This is particularly important from basic and translational research, as alterations in the deformability of the nucleus have been described in multiple human pathologies, including inflammation, aging, and cancer (12-14). It has been previously shown that three-dimensional (3D) in vitro confined environment compromises nuclear stability, promotes nuclear rupture and DNA damage, and perturbs different nuclear functions (15-18). However, it is not yet known how cell-environment interactions impact enduring alterations in the nucleus that drive genomic instability and cancer progression.

Here, we described how cell confinement endorses permanent changes that influence the mechanical and functional responses of the cell. We cultured leukemia cells embedded in a high-density 3D collagen-I matrix for several days. In terms of morphological and phenotypical changes, we demonstrate that 3D confinement induced nuclear swelling and lamin B1 redistribution. Moreover, we identified that actin polymerization and protein kinase C (PKC) activity cause lamin B1 redistribution in altered cells. Our transcriptional analysis reveals that transformed cells showed a different transcriptome compare to control cells. Importantly, we reveal that 3D confinement affected the biology of transformed cells in functions such as the migration, proliferation and survival. Finally, we combined atomic force microscopy (AFM), super resolution microscopy, confined compression, and optical tweezers, to demonstrate that transformed cells showed an homogeneous biomechanical signature inside the nucleus coupled to redistribution of chromatin. In summary, our results suggest that cell confinement can significantly impact nuclear changes, which could play a role in the regulation of other cell functions such as migration, transcription, and DNA repair.

MATERIAL AND METHODS

Cell culture. The human Jurkat (CVCL_0367) cell line was from ATCC, American Type Culture Collection. Jurkat cells were cultured in RPMI 1640 medium with L-glutamine, 25 mM HEPES

(Sigma), and 10% fetal bovine serum (Sigma) and maintained in 5% CO2 and 37ºC. TR cells were obtained upon long-term 3D confinement. For this, Jurkat cells were embedded in a solution of 3.3 mg/mL of collagen type I from bovine (Stem Cell) in complete medium and neutralized with 7.5% NaHCO3 and 25 mM Hepes. After 1 hour at 37ºC, extra additional complete medium was added at the top of the 3D collagen matrix. Jurkat cells were maintained in the 3D matrix for 10 days and the complete medium was changed every 3-4 days. Then, cells were collected from the collagen gel, cultured in suspension, and expanded as TR cells.

Immunofluorescence. Cells were cultured in suspension, treated or not with specific inhibitors at 37ºC. Cells were seeded onto 10 µg/mL poly-L-lysine-coated glass slides for 30 min. Then, cells were fixed with 4% formaldehyde for 10 min and permeabilized with 0.5% Triton x-100 (Tx-100) in PBS for 5 min. After 30 min blocking in 10% fetal bovine serum with 0.1% Tx-100 in PBS, samples were incubated with appropriate primary antibodies (1:100) for 1h at RT, followed by several PBS washes and 1h at RT incubation with secondary antibodies (1:200). Samples were stained with Hoechst 33342 1 µg/mL for 10 min at RT, washed with PBS and water, and mounted. Images were acquired on an inverted DMi8 microscope (Leica) using an ACS-APO 63x NA 1.30 glycerol immersion objective. Quantification and analysis of images were determined using ImageJ (National Institute Health). 3D reconstructions and videos were obtained by Leica software. For distribution analyses, lamin B1 signal from a cross-sectional plane of the cells was plotted and the mean of 15 cells was calculated and marked in red.

Nuclear isolation. Nuclei were isolated by resuspending cells in buffer A (10 mM HEPES, 10 mM KCl, 1.5 mM, $MgCl_2$, 0.34 M sucrose, 10% (v/v) glycerol, 1 mM DTT, 0.1% Tx100, and Roche protease inhibitor) for 5 min on ice. Following 3800 rpm centrifugation for 5 min, the pellet with the nuclei was resuspended in TKMC buffer (50 mM Tris pH 7.5, 25 mM KCl, 3 mM $MgCl_2$, 3 mM $CaCl_2$, and proteinase inhibitors) for conducting the indicated experiments.

Atomic Force Microscopy (AFM). AFM measurements were performed with a Bruker Bioscope Resolve mounted on an inverted microscope (Nikon Eclipse Ti2) connected to an ORCA-Flash4.0LT (Hamamatsu) camera. $8x10^5$ isolated nuclei from control and TR cells were seeded on 50 mm cell culture dishes (Willco GWST-5040) coated with 100 µg/mL PLL following the protocol in (19, 20). Imaging was performed in filtered PBS at room temperature. Pre-calibrated Silicon Tip – Nitride cantilevers (PFQNM-LC-V2 Bruker) were used with a 70 nm tip radius. PeakForce Tapping/PeakForce Capture with a maximum indentation force of 0.5 nN was used. Indentation curves were fitted within Nanoscope Analysis (Bruker) using a cone-sphere model (ADD) (21).

Nuclear mechanical compression. Isolated nuclei from cells were resuspended in TKMC buffer, dyed with Hoechst 33342 1 µg/mL and sedimented onto 10 µg/mL poly-L-lysine coated plates and placed in the cell confiner device (4D cell). Following the manufacturer's instructions, mechanical confinement was performed by pushing the nuclei with a glass slide with micropillars of 3 µm height. Images of at least 20 nuclei were taken with a 63× objective before and after the confinement by an

inverted confocal DMi8 microscope (Leica) and analysis of the nuclear area was performed with ImageJ.

Nuclear swelling stress. Isolated nuclei were resuspended in TKMC buffer and sedimented onto poly-L-lysine coated plates. Nuclei were incubated or not with 5 mM EDTA or KCl for 10 min. Then, nuclei were fixed, permeabilized, and stained with Hoechst 33342 (1 µg/mL). Quantification and analysis of nuclear area were determined using ImageJ software.

***In vivo* cell homing.** NOD-SCID-Il2rg-/- (NSG) mice (*Mus musculus*), were bred and maintained at the Servicio del Animalario del Centro de Investigaciones Biológicas Margarita Salas (CIB-CSIC) with number 28079-21A. All mice were used following guidelines issued by the European and Spanish legislations for laboratory animal care. Control and TR cells were labeled with Cell Tracker Far Red (2 µM) and CFSE (5 µM), respectively, for 30 min; then, cells were mixed 1:1 and $5x10^6$ mixture cells were injected intravenously (IV) in the tail vein of 9 weeks-old NSG mice. Animals were euthanized 24 hours after injection, and the bone marrow from femurs, spleens, and livers were extracted, processed through mechanical disaggregation, and resuspended in erythrocytes lysis buffer (150 mM NH_4Cl, 10 mM $KHCO_3$, 0.1 mM EDTA). Samples were acquired in a FacsCanto II (Beckton Dickinson) cytometer, and the percentage of labeled cells infiltrated into the tissues was analyzed using FlowJo software.

RESULTS

Prolonged cell confinement in 3D conditions promotes permanent morphological changes in the nucleus.

The size and morphology of the nucleus are critical for multiple homeostatic conditions, but also in human pathologies, such as cancer, where tumor cells show an abnormal morphology (22). First, we embedded leukemia cells (control) in 3D collagen gels and cultured them for 10 days. Then, transformed (TR) cells were collected from the 3D environment and cultured in suspension without any further physical constriction (**Figure 1A**). We visualized the nuclear morphology of control and TR cells and found that TR cells showed bigger nuclei than their counterparts (**Figure 1B, C**). We also confirmed the aberrant morphology, characterized by diminished nuclear circularity in TR cells (**Figure 1D**). In addition to confocal analysis, we analyzed the size and complexity of isolated nuclei from control and TR cells by flow cytometry. The distribution of both nuclear populations showed significant differences, confirming that isolated nuclei from TR cells presented bigger size and more complexity than those from control cells (**Figure 1E**). In order to further study the nuclear morphology, we assessed the morphological analysis of control and TR cells by electron microscopy (EM). TR cells exhibited a trend to present more and bigger nucleoli than control cells (**Suppl. Figure S1**). Furthermore, we also confirmed that TR cells showed an aberrant nuclear morphology compared to control cells (**Figure 1F**). Together, these results indicate that persistent confined environments induce permanent changes in the nucleus of TR cells.

Persistent 3D cell confinement alters the localization of lamin B1.

Lamin B1 is the major component of the nuclear lamina of lymphocytes (23). Since 3D confinement alters the size and morphology of TR cells, we hypothesized that lamin B1 distribution may also be affected in these cells. We visualized the nucleus of control and TR cells and found that lamin B1 localized in the nuclear periphery of control cells, whilst TR cells presented an aberrant distribution of this protein (**Figure 2A, 2B**). We further characterized differences in the morphology and lamin B1 distribution of nuclei from control and TR cells by performing 3D reconstruction (**Movie S1, S2**) and by visualizing aberrant lamin B1 invaginations in middle cross-section plane of TR cells (**Figure 2C**). It is well known that lamin B1 distribution is regulated by multiple kinases (24). We selectively inhibited conventional PKC activity with staurosporine (for PKCα) and enzastaurin (for PKCβ) and found that PKCβ inhibition suggested a partial recovery of the normal lamin B1 distribution in TR cells (**Suppl. Figure S2**). To demonstrate this, we transfected TR cells with the specific siRNA against PKCβ (**Suppl. Figure S2**) and studied the distribution of lamin B1. As we anticipated, lamin B1 localized in the nuclear periphery in PKCβ-depleted cells (**Figure 2D, 2E**), confirming that PKC activity is required for this nuclear alteration induced by cell confinement. Together, our results indicate that transformed cells by 3D confined environments alter the localization of lamin B1 through the activation of PKCβ.

Actin polymerization modulates the aberrant distribution of lamin B1.

The cytoskeleton mediates mechanical signals between cells and their surrounding environment (25-27). We addressed the potential implication of actin polymerization on the aberrant distribution of lamin B1 in TR cells. We incubated TR cells with chemical drugs to target actin polymerization and found that latrunculin B (an actin polymerization inhibitor) treatment promoted the localization of lamin B1 at the nuclear periphery (**Figure 3A, 3B**). In contrast to latrunculin, pharmacological treatment with jasplakinolide, which stabilizes polymerized actin, did not significantly alter the distribution of lamin B1 (**Figure 3A, 3B**). It has been reported that nuclear actin and its associated proteins play fundamental nuclear functions, such as chromatin changes, DNA repair and transcriptional regulation (28). To further characterize the role of actin polymerization on the aberrant distribution of lamin, we transfected mutants of nuclear actin in TR cells and evaluated their nuclear phenotype. We confirmed that transfected cells with R actin (an inactive mutant for actin polymerization) rescued in TR cells the phenotype observed in control cells; nonetheless, the S actin (a mutant that recapitulates the effect of jasplakinolide) did not significantly alter the distribution of lamin B1 (**Figure 3C, 3D**). As blocking actin polymerization and PKCβ signaling recovered the normal distribution of lamin B1, we interrogated which molecular mechanism was the primary signal controlling this nuclear change in TR cells. For this, we incubated TR cells with PMA (Phorbol 12-myristate 13-acetate) to stimulate the activation of PKC and observed that PMA treatment did not abrogate the effect of latrunculin on TR cells (**Suppl. Figure S3**). Furthermore, we treated TR cells depleted for PKCβ or preincubated with enzastaurin with jasplakinolide and found that actin

stabilization overcame the recovery induced by targeting PKCβ (**Figure 3E, 3F**). When we inverted the order and pretreated TR cells with jasplakinolide before the addition of enzastaurin, we confirmed that actin stabilization also impaired the effect induced by PKC inhibition (**Suppl. Figure S3**). Taken together, these results suggest that actin polymerization regulates the distribution of lamin B1 in TR cells, and this effect might operate downstream the PKC signaling.

Aberrant cells after suffering 3D confinement alter their transcriptional program.

It has been recently published that 3D collagen matrix density promotes cell fate transition in fibroblasts (29). As the actin cytoskeleton and an aberrant nuclear morphology are linked to the transcriptional activity of the cell (30), we interrogated whether these nuclear changes induced by 3D conditions were subsequent to gene expression alterations in TR cells. Our microarray expression analysis showed a significant differential expression of 1.4-fold change in 661 genes (143 up- and 518 down-regulated) in TR cells compared with control cells (**Figure 4A, 4B**). We performed bioinformatics analysis of the gene expression profiles in control and TR cells and found that the most significant changes correspond to genes encoding mitochondrial transport, cytokine signaling and extracellular matrix organization pathways (**Figure 4C, Suppl. Figure S4, and Table S1**). In order to validate our data, we selected two genes related to leukemia biology and determined their levels by RT-qPCR. Consistent with our transcriptional analysis, the levels of *MEN1* and *EHMT2* were diminished in TR cells (**Suppl. Figure S4**). Then, we interrogated how 3D matrix environment might promote different transcriptional changes at short-term and in the TR cells. For this, we cultured cells in suspension or embedded in a 3D collagen matrix for 3h, and then analyzed their transcriptional activity, observing that cells cultured at short-times in 3D conditions also altered their transcriptional profile (**Figure 4D, Suppl. Figure S4, Suppl. Table S2**). Furthermore, when we compared short- and long-time situations, we found that only 38 genes were altered in cells cultured for 3h in 3D conditions and in TR cells (**Figure 4E, and 4F Suppl. Table S3**); indicating that prolonged confinement promotes different outputs in the cell biology than short-term conditions. Together, these results demonstrate that persistent confinement in 3D environments promotes enduring changes in the transcriptional signature of cells.

Persistent 3D cell confinement causes cell cycle and survival alterations

Confined conditions regulate the proliferation and cell cycle progression of cells (31, 32). Thereby, we investigated whether TR cells may present differences in their proliferative ratio. We found that the proliferative ratio of TR cells showed a slight reduction compared to control cells (**Figure 5A**). By analyzing the BrdU (bromodeoxyuridine) incorporation, we found no significant differences in the capacity of TR cells to divide (**Figure 5B**). Furthermore, we analyzed the cell cycle progression of control and TR cells and observed a minor effect of TR cells to accumulate in the G1 phase (**Suppl. Figure S5**). To further confirm these findings, we tested the expression of cyclins and found that TR cells exhibited diminished levels of cyclin A (a typical cyclin for late-phases of the cell cycle) compared to control cells (**Suppl. Figure S5**). Cell migration through confined spaces compromises

nuclear integrity and promotes DNA damage (33). To determine how DNA damage might be connected to persistent 3D confined conditions, we visualized γH2AX, a well-known DNA damage marker (34), and found that TR cells showed higher number of cells with more than 8 foci of γH2AX per nucleus than control cells (**Figure 5C, 5D**). As we found high levels of this DNA damage marker in TR cells, we characterized their DNA repair response by treating control and TR cells with bleomycin, a drug that induces DNA damage. We visualized the levels of DNA damage by single-cell electrophoresis (comet assay) and found that TR cells were more sensitive to DNA damage than control cells (**Figure 5E, 5F and Suppl. Figure S5**). Moreover, given the potential implication of the basal levels of DNA damage response on the survival capacity of the cells, we tested whether TR cells were more sensitive to conventional chemotherapies than control cells. Interestingly, we confirmed that TR cells showed more sensitivity to cell death in response to several chemotherapeutic drugs than control cells (**Figure 5G and Suppl. Figure S5**). Together, our results suggest that during persistent 3D confinement, cells undergo permanent changes that alter their proliferative and apoptotic responses.

Aberrant cells after suffering 3D confinement exhibit reduced cell invasiveness.

To determine other functions altered in TR cells, we evaluated their migration efficiency. Firstly, we performed a transwell migration assay and found that TR cells showed a defective migration in response to serum (**Figure 6A**). To discard that differences in chemotaxis may be regulated by defective cell adhesion, we evaluated the adhesion of control and TR cells to VCAM-1 (vascular adhesive molecule-1). We did not observe any difference in the levels of TR cells attached to VCAM-1 (**Suppl. Figure S6**). To further determine the migration of TR cells in vitro, we analyzed their capacity to infiltrate into a collagen matrix and found that the deepness invasion of TR cells was not impaired (**Figure 6B and 6C**). Then, we assessed how TR cells might have altered their invasive capacity in vivo. For this, we injected an equal number of control and TR cells labelled with vital dyes into the tail vein of immunodeficient recipient mice and analyzed the homing of cells into the bone marrow, liver, and spleen at 24h post-injection. Our analysis indicated a reduction of TR cells reaching these organs compared to controls (**Figure 6D and Suppl. Figure S6**). Together, these results indicate that cell confinement at long-term reduces the capacity of TR cells to invade and reach other tissues.

Persistent 3D confinement modulates nuclear biophysics and homogeneity.

Nuclear deformability is critical during cell migration through physical barriers such as the endothelium and the interstitial spaces (35, 36). Since the nuclear size and morphology of TR cells were affected, we hypothesized that the nuclear deformability would be also affected. To determine how the nucleus deforms upon external forces, we used a cell confiner device, to induce nuclear deformation by global compression. We found that isolated nuclei from TR cells increased their nuclear deformability compared to isolated nuclei from control cells, indicating that persistent cell confinement indeed may affect the mechanical response of the nucleus (**Figure 7A, 7B**). The

chromatin compaction also contributes to the mechanical properties of the nucleus (19), and we first interrogated whether TR cells alter their chromatin organization. We assessed DNAse I sensitivity assay to determine the global chromatin compaction of control and TR cells. We found that TR cells exhibited more sensitivity to DNA digestion than control cells, suggesting a more relaxed chromatin compaction (**Figure 7C, 7D**). To further explore this possibility, we treated control and TR cells with trichostatin A (TSA), a chemical drug to induce chromatin decompaction. We revealed that TSA treatment increased significant the nuclear size of control cells, while TR cells were less sensitive to this treatment, indicative of lower levels of chromatin compaction than control cells (**Figure S7**). To investigate these changes in chromatin, we used STORM (Stochastic Optical Reconstruction Microscopy) imaging to observe the spatial organisation and density of chromatin within isolated nuclei. As shown in **Figure 7E**, we observed a high density of chromatin stained by SiR-DNA around the periphery of the nucleus in control nuclei. TR nuclei displayed an altered chromatin distribution with a decrease in peripheral density and an increase in staining within the nuclear body. SIM (Structured Illumination Microscopy) imaging was used to observe the spatial organisation of chromatin within whole cells (**Figure 7E**). These images are consistent with the altered chromatin staining observed using STORM, which confirms isolation of the nuclei does not alter chromatin organization. Overall, the staining is similar to the distribution of Lamin B within both cell lines observed in **Figure 2A**, which suggests a potential link between the lamina and chromatin organisation, along with accessibility. Osmotic stress has been used to determine the mechanical response of the nucleus (37), as swelling conditions might affect the chromatin compaction and the water diffusivity inside the nucleus. We added KCl or EDTA to isolated nuclei from control and TR cells to determine how the nucleus might respond to swelling conditions. We observed that both treatments increased the area of isolated nuclei from control and TR cells. To address whether actin polymerization might influence on these differences, we treated TR cells with latrunculin and found that these isolated nuclei showed a nuclear swelling more similar to control cells (**Figure S7**). We also confirmed that latrunculin treatment reduced the chromatin sensitivity of TR cells to the enzymatic activity of DNAse (**Figure S7**).

Consequently, the aberrant lamin B distribution observed in the TR cells might be linked to alterations on the chromatin organization. We reasoned that the complex set of interactions governing the NE-chromatin crosstalk is encoded as a compaction gradient extending from the nuclear lamina towards the inner nuclear regions (38). Therefore, we hypothesized that this sort of alterations should be also projected as permanent remodelling effects over the isolated nuclear structure. In this sense, we have developed a methodology based on gentle poroelastic indentation using optical tweezers that enables the estimation of the nuclear local density (compaction) for a certain indentation depth, by merging the information from stiffness and characteristic time of the force relaxation. We applied a range of indentation depths in both isolated nuclei from control and TR cells to reveal the spatial variation of the compaction at the nuclear periphery and found an exponential decay defined by a shape factor of

the function, named characteristic length XI (**Figure 7F**). Although we did not observe significant differences between the average XI values (**Fig. S8**), we evinced a noticeable difference in the data dispersion being larger in the TR phenotype (**Figure 7F**), which might indicate that the compaction gradient at the nuclear periphery is more heterogeneous in the TR cells. To further characterize the spatial biomechanical signature of TR cells, we used AFM on isolated nuclei (39). Using PeakForce Capture and PeakForce Tapping, we are able to gain a force curve for each pixel (**Figure 7G**); therefore, we can measure the spatial biomechanical properties. We found that control nuclei are an inhomogeneous material with distinct islands of high stiffness, whilst TR nuclei display a homogeneous stiffness across the nucleus (**Figure 7G**). In this manner, the underlying alterations within the TR cells correlated with a change in the mechanical properties. Calculating the mean stiffness for the nuclei, we could observe an increase in stiffness within the TR nuclei (**Figure 7H**). The increase in stiffness was consistent with a redistribution of lamina and chromatin, which are significant contributing factor to nuclear mechanics. Taken together, our findings indicate that prolonged cell confinement in 3D conditions leads to global changes in the chromatin compaction and biomechanical signature of the nucleus.

DISCUSSION

Cell migration is a multistep process where migratory cells have to respond to external stimuli to alter their molecular and biophysical properties in order to cross extracellular barriers such as endothelia or the extracellular matrix (7, 26, 40). These mechanical constraints suffered by cells control multiple processes related to homeostatic and pathological conditions, including proliferation, apoptosis, tumorigenesis, and cell fate transitions. Here, we described a number of nuclear alterations due to cell culture in 3D environmental conditions; some of them related to morphological and functional changes of the cell, others connected to the chromatin impact and mechanical behaviour of the nucleus.

It is known that the nucleus of migratory cells presents temporary changes during constrained migration. These changes include the mechanical response, nuclear blebs at the leading edge, or even the rupture of the nucleus (17, 18, 41-43). It was already known that 3D migration controls chromatin changes and alters the transcriptional activity of migratory cells that might persist for days (33); however, how 3D culture conditions promote permanent changes in the nucleus of the cell is not fully understood. In this study, we observed that confined cell culture led to permanent phenotypical changes. Under control conditions, cells exhibit normal nuclear morphology and nucleoli. Nonetheless, TR cells exhibited a more aberrant nuclear shape, concomitant with more nucleoli. It has been described that the number of nucleoli is connected with a more invasive phenotype of cancer cells (44, 45). Furthermore, the aberrant nuclear morphology serves as a pathological marker for cancer cells (46). Therefore, it is possible that 3D constraints might generate physical stress that favors cancer heterogeneity and chromatin instability.

Aberrant nuclear morphology usually enrols alterations of the nuclear envelope and chromatin changes that may contribute to pathological conditions and cancer progression. Aligning with this, it has been demonstrated that breast carcinoma cells cultured on nanopillars alter their subnuclear morphologies and the distribution of lamin A, concomitant with higher malignancy and cell migration (46). This is particularly important as the lamina network provides the mechanical skeleton to the nucleus, and the levels and the regulation of lamins alter the biomechanical response of the nucleus, the chromatin organization, and the transcriptional activity (2, 5, 32). While lamin A might be found in the nucleoplasm, most of lamin B1 localizes at the nuclear periphery. Phenotypically, our data indicate that cell confinement in 3D induces lamin B1 redistribution in TR cells. Changes in the localization or distribution of lamin B might be of particular interest, due to lamin-A type levels, but not lamin B, reflect changes in the mechanical properties of the nucleus (47). Thus, our data suggest that the specific localization of lamin B might play important role in regulating nuclear alterations. Lamin B1 alters its distribution during the cell cycle and might suffer phosphorylation by multiple kinases (48). Consistent with the idea that PKC activity control lamin B distribution, our findings show that blocking or silencing PKCβ recovers the normal distribution of lamin B at the nuclear periphery. Accordingly, we found that latrunculin treatment also abrogates the aberrant distribution of lamin B in TR cells. One of the key cellular regulators of nuclear dysmorphia, lamin redistribution and chromatin changes is actomyosin contractility (49). In addition, the actin cytoskeleton connects the cell receptors to the nuclear envelope and leads to the transmission of external stimuli, nuclear translocation, and other intracellular pathways that control the mechanical response of the nucleus (50). Apart from their role in the cytoplasm, the actomyosin machinery (actin, myosins, and associated proteins) can be recruited into the nucleus interacting with polymerases and transcription factors regulating multiple functions, including DNA repair, transcription, and cell cycle progression (27, 51, 52). Here, we demonstrated that nuclear actin controls the lamin B1 redistribution in TR cells. Furthermore, when we interrogated whether latrunculin treatment may regulate lamin redistribution downstream of PKC activity, we found that actin operates connected and downstream of PKC, as the disruption of actin polymerization bypasses the effect of PKC. The reasons for these remain unclear and continued studies are needed to better understand specific functions of nuclear actin and PKC isoforms, and how 3D cell culture might contribute to the activation and these molecular processes.

The mechanical stress controls the transcriptional activity of the cell (10, 53, 54). Recent evidence demonstrates that cell growth of human fibroblasts on geometric constraints alters the transcriptional program of the cell and induces cell-fate transitions (28). These changes induced during the lateral confinement in geometric micropatterns are mainly mediated by Lef1 signaling (55). It has been recently proposed that confined migration through narrow spaces might advantage both the selection and induction of phenotypical changes similar to the metastatic process; however, these mechanisms might differ between microfluid devices and 3D matrices (35). We have identified a set of transcriptional changes in TR cells that might be involved in their cell cycle progression, DNA

damage response, and the ability to penetrate and invade other tissues. Previous reports have demonstrated that the two major contributors to the DNA repair and DNA damage response (DDR) pathways, ATM and ATR, have been involved in the nuclear mechanics and lamin disposition during cancer cell migration (56, 57). We observed that TR cells showed more H2AX foci in resting conditions, suggesting that these cells might suffer higher genomic stress and a predisposition to become more sensitive to specific treatments. By treating TR cells with different drugs used in clinics to target leukemia progression, we found that these cells were more sensitive to most of these treatments than untransformed control cells. This might suggest that nuclear changes induced by 3D conditions might alter the basal levels of DNA damage markers and the efficiency of therapies against cancer dissemination. On the other hand, these changes might also have a significant impact on genome integrity, leading to heterogeneity and triggering the escape of certain clones or mutations. In turn, genome instability is an effect induced by confined conditions and cell constrainment (58, 59). We cannot rule out the possibility that this might be connected to different transcriptional activity and long-term adaptive response of TR cells to 3D conditions and further studies should be directed to address the transcriptional and functional consequences of 3D conditions in cancer cells.

The chromatin structure and organization depend on its interaction with packing proteins, with lamins and other supramolecular structures, such as chromosomal territories (60). The genomic dynamics contribute to the mechanical properties of the nucleus and the cell capacity to squeeze and migrate through narrow spaces. Preventing chromatin changes resulted in impaired migration of multiple cell types through confined conditions (16, 35, 36). We found that TR cells showed less compacted chromatin, which results in more sensitivity nucleosomes to DNAse activity, and redistributed around the nucleus in a manner similar to the redistribution of lamin B. The effect of TSA on nuclear size and chromatin compaction has been studied previously (34). In agreement with these studies and our observations using DNAse, TR cells showed a minor nuclear expansion under TSA treatment, indicating a lower chromatin compaction *per se*. It is plausible that the less condensed chromatin of TR cells might be a key factor to prime these cells for different nuclear functions. This might be particularly important as chromatin changes observed in microfluidic devices might not operate in 3D collagen matrices (35). As both, the chromatin and the nuclear lamina disposition seemed to be altered in TR cells, we assessed how 3D confined conditions might promote persistent changes in the mechanical signature of the nucleus. There are multiple biophysical techniques to promote and study the deformation of the nucleus (61). As each of these methods perturbs the nucleus differently, the use of complementary approaches provides a more comprehensive view of the biophysical signature of the nucleus. First, we observed by optical tweezers that the abnormal lamin distribution found in TR cells might be linked to a more heterogeneous chromatin compaction at the nuclear periphery. This heterogeneity might be due to the force balance at the nuclear edge. In general terms, the spheroidal shape of the cell nucleus is defined by the mechanical balance between the osmotic pressure (outwards) and the Laplace pressure (inwards), which is defined by the mechanical stress at the

interface (62). As a consequence, it is expected that a more compact and homogeneous periphery would define a nuclear structure without geometrical heterogeneities, as observed in the control nuclei. Conversely, the existence of regions with a weakened surface tension can rise to the formation of mechanical instabilities as those observed in nuclear blebs or in laminopathies (63). When we used a specific AFM approach to identify the continuum biophysical signature of isolated nuclei, we showed that aberrant nuclei from TR cells present an increased stiffness, which correlates with morphological alterations and changes in the DNA susceptibility to enzymatic degradation. It has been reported how AFM and another mechanical techniques differ considerably in the quantified response (36, 64, 65). Our results suggest that the differences between the nuclear compression, AFM and optical tweezers might be likely due to more complex factors contributing to the mechanical response of the nucleus, including a higher level of chromatin decondensation, diminution of actin polymerization, and loosening of the nuclear lamina, which is an interesting difference that will need further studies in the future.

Overall, our findings describe how 3D cell culture conditions promote a variety of persistent nuclear alterations on various scales, including morphology, chromatin conformation, lamin distribution, and the biomechanical response of the nucleus. Considering the functional changes observed in gene expression, the biophysical properties, and the migration of TR cells in vitro and into xenograft in vivo models; our observations may contribute to explaining novel biomechanical effects of 3D conditions in the nuclear biology that might occur during cancer cell invasion, tissue repair, and developmental processes.

DATA AVAILABILITY

Microarray data have been deposited with the Gene Ontology Database under accession numbers GSE181375 and GSE226621. All relevant data are available from the corresponding author upon reasonable request.

ETHICS APPROVAL

All procedures for animal experiments were approved by the Committee on the Use and Care of Animals and carried out in strict accordance with the institution guidelines and the European and Spanish legislations for laboratory animal care.

SUPPLEMENTARY DATA

Supplementary Data are available at NAR online.

AUTHOR CONTRIBUTIONS

R.G.N., H.Z.C., conducted experiments and contributed to data interpretation and discussion. A.D.L., conducted experiments and contributed to data interpretation. H.L.M. conducted experiments and

contributed to data interpretation. P.R.N., F.M. supervised the experiments related to the optical tweezers, contributed to data interpretation and provided financing. L.W., designed and supervised the experiments related to STORM. C.P.T., designed and supervised the experiments related to STORM and AFM, contributed to data interpretation, and provided financing. J.R.M designed and supervised the experiments, contributed to data interpretation, wrote the paper, and provided financing.

ACKNOWLEDGEMENT

The authors thank the Microscopy Unit of Instituto de Investigación Biosanitaria Gregorio Marañón (IiSGM) for assistance with confocal analyses. The authors are also grateful to the EM and Animal Facilities of platforms of the CIB Margarita Salas for their assistance and support with the EM and in vivo experiments. The UCM-Genomic CAI Unit for their assistance with microarray experiments. We thank Robert Moorhead and Daniel. E. Rollins for assistance and support at Royce@Sheffield.

FUNDING

We wish to acknowledge the Henry Royce Institute for Advanced Materials, funded through Engineering and Physical Sciences Research Council (EP/R00661X/1, EP/S019367/1, EP/P02470X/1 and EP/P025285/1). This research was supported by a FPI Scholarship 2018 (Ministerio de Ciencia e Innovación/MICINN, Agencia Estatal de Investigación/AEI y Fondo Europeo de Desarrollo Regional/FEDER) to R.G.N.; grants from Comunidad de Madrid (Y2018/BIO-5207) and from the Ministerio de Ciencia e Innovación (MICINN) Agencia Estatal de Investigación (AEI) (PID2020-115444GB-I00) to P.R.N; grants from the Ministerio de Ciencia e Innovación (MICINN) Agencia Estatal de Investigación (AEI) (PID2019-108391RB-100), and Comunidad de Madrid (Y2018/BIO-5207, S2018/NMT-4389 and REACT-EU program PR38-21-28 ANTICIPA-CM) to F.M.; Medical Research Council (MR/M020606/1) and Science and Technology Facilities Council (19130001) to C.P.T.; and grants from 2020 Leonardo Grant for Researchers and Cultural Creators (BBVA Foundation), Ayuda de contratación de ayudante de investigación PEJ-2020-AI/BMD-19152 (Comunidad de Madrid), and the Ministerio de Ciencia e Innovación (MICINN) Agencia Estatal de Investigación (AEI) (PID2020-118525RB-I00) to J.R.M.

CONFLICT OF INTEREST

Authors declare no conflict of interest.

REFERENCES

1. Carollo, P.S., and Barra, V. (2023) Chromatin epigenetics and nuclear lamina keep the nucleus in shape: Examples from natural and accelerated aging. *Biol. Cell.* **115**, e2200023.

2. Burke, B., and Stewart, C.L. (2013) The nuclear lamins: flexibility in function. *Nat. Rev. Mol. Cell Biol.* **14**, 13–24.

3. Cho, S., Irianto, J., and Discher, D.E. (2017) Mechanosensing by the nucleus: From pathways to scaling relationships. *J. Cell Biol.* **216**, 305–315.

4. Dahl, K.N., Ribeiro, A.J., and Lammerding, J. (2008) Nuclear shape, mechanics, and mechanotransduction. *Circ. Res.* **102**, 1307–1318.

5. Stephens, A.D., Banigan, E.J., Adam, S.A., Goldman, R.D. and Marko, J.F. (2017) Chromatin and lamin A determine two different mechanical response regimes of the cell nucleus. *Mol. Biol. Cell,* **28**, 1984–1996.

6. Lammerding, J., Engler, A.J., and Kamm, R. (2022) Mechanobiology of the cell nucleus. *APL Bioeng.* **6**, 040401.

7. Mierke, C.T. (2019) The matrix environmental and cell mechanical properties regulate cell migration and contribute to the invasive phenotype of cancer cells. *Rep. Prog. Phys.* **82**, 064602.

8. Jung-Garcia, Y., Maiques, O., Monger, J., Rodriguez-Hernandez, I., Fanshawe, B., Domart, M.C., Renshaw, M.J., Marti, R.M., Matias-Guiu, X., Collinson, L.M., Sanz-Moreno, V., and Carlton, J.G. (2023) LAP1 supports nuclear adaptability during constrained melanoma cell migration and invasion. *Nat. Cell Biol.* **25**, 108-119.

9. Alisafaei, F., Jokhun, D.S., Shivashankar, G.V., and Shenoy, V.B. (2019). Regulation of nuclear architecture, mechanics, and nucleocytoplasmic shuttling of epigenetic factors by cell geometric constraints. *Proc. Natl. Acad. Sci. USA* **116**, 13200–13209

10. Damodaran, K., Venkatachalapathy, S., Alisafaei, F., Radhakrishnan, A.V., Sharma Jokhun, D., Shenoy, V.B., and Shivashankar, G.V. (2018) Compressive force induces reversible chromatin condensation and cell geometry–dependent transcriptional response. *Mol. Biol. Cell* **29**, 3039–3051.

11. Guilluy, C., Osborne, L.D., Van Landeghem, L., Sharek, L., Superfine, R., Garcia-Mata, R., and Burridge, K. (2014). Isolated nuclei adapt to force and reveal a mechanotransduction pathway in the nucleus. *Nat. Cell Biol.* **16**, 376–381.

12. Pickup, M.W., Mouw, J.K., and Weaver, V.M. (2014) The extracellular matrix modulates the hallmarks of cancer. *EMBO Rep.* **15**, 1243–53.

13. Zhong, J., Yang, Y., Liao, L., and Zhang, C. (2020) Matrix stiffness-regulated cell functions under different dimensionalities. *Biomater. Sci.* **8**, 2734–55.

14. Wullkopf, L., West, A.K.V., Leijnse, N., Cox, T.R., Madsen, C.D., Oddershede, L.B., and Erler, J.T. (2018) Cancer cells' ability to mechanically adjust to extracellular matrix stiffness correlates with their invasive potential. *Mol. Biol. Cell.* **29**, 2378–85.

15. Engler, A.J., Sen, S., Sweeney, H.L., and Discher, D.E. (2006) Matrix elasticity directs stem cell lineage specification. *Cell* **126**, 677–689.

16. Wang, P., Dreger, M., Madrazo, E., Williams, C.J., Samaniego, R., Hodson, N.W., Monroy, F., Baena, E., Sanchez-Mateos, P., Hurlstone, A., and Redondo-Munoz, J. (2018) WDR5 modulates cell motility and morphology and controls nuclear changes induced by a 3D environment. *Proc. Natl. Acad. Sci. USA* **115**, 8581–8586

17. Raab, M., Gentili, M., de Belly, H., Thiam, H.R., Vargas, P., Jimenez, A.J., Lautenschlaeger, F., Voituriez, R., Lennon-Dumenil, A.M., Manel, N., et al. (2016) ESCRT III repairs nuclear envelope ruptures during cell migration to limit DNA damage and cell death. *Science* **352**, 359–362.

18. Denais, C.M., Gilbert, R.M., Isermann, P., McGregor, A.L., te Lindert, M., Weigelin, B., Davidson, P.M., Friedl, P., Wolf, K., and Lammerding, J. (2016). Nuclear envelope rupture and repair during cancer cell migration. *Science* **352**, 353–358.

19. Dos Santos, Á., Cook, A.W., Gough, R.E., Schilling, M., Olszok, N.A., Brown, I., Wang, L., Aaron, J., Martin-Fernandez, M.L., Rehfeldt, F., and Toseland, C.P. (2021) DNA damage alters nuclear mechanics through chromatin reorganization. *Nucleic Acids Res.* **49**, 340-353.

20. Dos Santos, A. Gough, R.E., Wang, L., and Toseland, C.P. (2022) Measuring Nuclear Organization of Proteins with STORM Imaging and Cluster Analysis. Chromosome Architecture. *Methods in Molecular Biology* **2476**, 293-309.

21. Brisco, B.J., Sebastian, K.S., Adams M.J. (1994) The effect of indenter geometry on the elastic response to indentation. *J. Phys. D: Appl. Phys.* **27,** 1156-1162.

22. Radhakrishnan, A., Damodaran, K., Soylemezoglu, A. C., Uhler, C., and Shivashankar, G.V. (2017) Machine Learning for Nuclear Mechano-Morphometric Biomarkers in Cancer Diagnosis. *Sci. Rep.* **7**, 17946.

23. Röber, R.A., Sauter, H., Weber, K., and Osborn, M. (1990) Cells of the cellular immune and hemopoietic system of the mouse lack lamins A/C: distinction versus other somatic cells. *J. Cell Sci.* **95**, 587-98.

24. Torvaldson, E., Kochin, V., and Eriksson, J.E. (2015) Phosphorylation of lamins determine their structural properties and signaling functions. *Nucleus* **6**, 166 –171

25. Lammerding, J., and Wolf, K. (2016). Nuclear envelope rupture: actin fibers are putting the squeeze on the nucleus. *J. Cell Biol.* **215**, 5–8.

26. Buxboim, A., Swift, J., Irianto, J., Spinler, K.R., Dingal, P.C.D.P., Athirasala, A., Kao, Y.-R.C., Cho, S., Harada, T., Shin, J.W., and Discher, D.E. (2014) Matrix elasticity regulates lamin-A, C phosphorylation and turnover with feedback to actomyosin. *Curr. Biol.* **24**, 1909–1917.

27. Yamazaki, D., Kurisu, S., Takenawa, T. (2005) Regulation of cancer cell motility through actin reorganization. *Cancer Science.* **96**,379–386.

28. de Lanerolle, P. (2012) Nuclear actin and myosins at a glance. *J. Cell Sci.* **125**, 4945–4949.

29. Roy, B., Yuan, L., Lee, Y., Bharti, A., Mitra, A., and Shivashankar, G.V. (2020) Fibroblast rejuvenation by mechanical reprogramming and redifferentiation. *Proc. Natl. Acad. Sci. USA* **117**, 10131-10141.

30. Gupta, S., Marcel, N., Sarin, A., and Shivashankar, G.V. (2012) Role of actin dependent nuclear deformation in regulating early gene expression. *PLoS One* **7**, e53031.

31. Tilghman, R.W., Cowan, C.R., Mih, J.D., Koryakina, Y., Gioeli, D., Slack-Davis, J.K., Blackman, B.R., Tschumperlin, D.J., and Parsons, J.T. (2010) Matrix rigidity regulates cancer cell growth and cellular phenotype. *PLoS One.* **5**, e12905.

32. Streichan, S.J., Hoerner, C.R., Schneidt, T., Holzer, D., and Hufnagel, L. (2015) Spatial constraints control cell proliferation in tissues. *Proc. Natl. Acad. Sci. USA* **111**, 5586-91.

33. Cho, S., Vashisth, M., Abbas, A., Majkut, S., Vogel, K., Xia, Y., Ivanovska, I.L., Irianto, J., Tewari, M., Zhu, K., et al. (2019) Mechanosensing by the Lamina Protects against Nuclear Rupture, DNA Damage, and Cell-Cycle Arrest. *Dev. Cell* **49**, 920-935.e5.

34. Paull,T.T., Rogakou,E.P., Yamazaki,V., Kirchgessner,C.U., Gellert,M. and Bonner,W.M. (2000) A critical role for histone H2AX in recruitment of repair factors to nuclear foci after DNA damage. *Curr. Biol.,* **10**, 886–895.

35. Kalukula, Y., Stephens, A.D., Lammerding, J., and Gabriele, S. (2022) Mechanics and functional consequences of nuclear deformations. *Nat. Rev. Mol. Cell Biol.* **23**, 583-602.

36. Hsia, C.R., McAllister, J., Hasan, O., Judd, J., Lee, S., Agrawal, R., Chang, C.Y., Soloway, P., and Lammerding, J. (2022) Confined migration induces heterochromatin formation and alters chromatin accessibility. *iScience.* **25**, 104978.

37. Zhang, X., Cook, P.C., Zindy, E., Williams, C.J., Jowitt, T.A., Streuli, C.H., MacDonald, A.S., and Redondo-Muñoz, J. (2016). Integrin a4b1 controls G9a activity that regulates epigenetic changes and nuclear properties required for lymphocyte migration. *Nucleic Acids Res.* **44**, 3031–3044.

38. Le Gros, M.A., Clowney, E.J., Magklara, A., Yen, A., Markenscoff-Papadimitriou, E., Colquitt, B., Myllys, M., Kellis, M., Lomvardas, S., Larabell, C.A. (2016) Soft X-Ray tomography reveals gradual chromatin compaction and reorganization during neurogenesis in vivo. *Cell Rep.* **17**, 2125-2136.

39. Lherbette, M., dos Santos, A., Hari-Gupta, Y., Fili, N., Toseland, C.P. and Schaap, I.A.T. (2017) Atomic Force Microscopy micro-rheology reveals large structural inhomogeneities in single cell-nuclei. *Sci. Rep.,* **7**, 8116.

38. Lautscham, L.A., Kammerer, C., Lange, J.R., Kolb, T., Mark, C., Schilling, A., Strissel, P.L., Strick, R., Gluth, C., Rowat, A.C., et al. (2015). Migration in confined 3D environments is determined by a combination of adhesiveness, nuclear volume, contractility, and cell stiffness. *Biophys. J.* **109**, 900–913.

39. Paul, C.D., Mistriotis, P., and Konstantopoulos, K. (2017) Cancer cell motility: lessons from migration in confned spaces. *Nat. Rev. Cancer* **17**, 131–140.

40. Shah, P., Hobson, C.M., Cheng, S., Colville, M.J., Paszek, M.J., Superfine, R., and Lammerding, J. (2021) Nuclear deformation causes DNA damage by increasing replication stress. *Curr. Biol.* **31**, 753–765.e6.

41. Irianto, J., Xia, Y., Pfeifer, C.R., Athirasala, A., Ji, J., Alvey, C., Tewari, M., Bennett, R.R., Harding, S.M., Liu, A.J., et al. (2017) DNA damage follows repair factor depletion and portends genome variation in cancer cells after pore migration. *Curr. Biol.* **27**, 210–223.

42. Xia, Y., Ivanovska, I.L., Zhu, K., Smith, L., Irianto, J., Pfeifer, C.R., Alvey, C.M., Ji, J., Liu, D., Cho, S., et al. (2018). Nuclear rupture at sites of high curvature compromises retention of DNA repair factors. *J. Cell Biol.* **217**, 3796–3808.

43. Montanaro, L., Treré, D., and Derenzini, M. (2008) Nucleolus, ribosomes, and cancer. *Am. J. Pathol.* **173**, 301–310.

44. Derenzini, M., Montanaro, L., and Treré, D. (2009) What the nucleolus says to a tumour pathologist. *Histopathology*. **54**, 753-62.

45. Yu, K.-H., Zhang, C., Berry, G.J., Altman, R.B., Ré, C., Rubin, D.L., and Snyder, M. (2016) Predicting non-small cell lung cancer prognosis by fully automated microscopic pathology image features. *Nat. Commun.* **7**, 12474.

46. Zeng, Y., Zhuang, Y., Vinod, B., Guo X, Mitra A, Chen P, Saggio I, Shivashankar GV, Gao W, Zhao W. (2022). Guiding Irregular Nuclear Morphology on Nanopillar Arrays for Malignancy Differentiation in Tumor Cells. *Nano Lett.* **22**, 7724-7733.

47. Lammerding, J., Fong, L.G., Ji, J.Y., Reue, K., Stewart, C.L., Young, S.G., and Lee, R.T. (2006) Lamins A and C but not lamin B1 regulate nuclear mechanics. *J. Biol. Chem.* **281**, 25768–25780.

48. Ottaviano, Y., and Gerace, L. (1985) Phosphorylation of the nuclear lamins during interphase and mitosis. *J. Biol. Chem.* **260**, 624–632.

49. Takaki, T., Montagner, M., Serres, M.P., Le Berre, M., Russell, M., Collinson, L., Szuhai, K., Howell, M., Boulton, S.J., Sahai, E., and Petronczki, M. (2017) Actomyosin drives cancer cell nuclear dysmorphia and threatens genome stability. *Nat. Commun.* **8**, 16013.

50. Han, T., Jiang, Y., Wang, X., Deng, S., Hu, Y., Jin, Q., Long, D., and Liu, K. (2022) 3D matrix promotes cell dedifferentiation into colorectal cancer stem cells via integrin/cytoskeleton/glycolysis signaling. *Cancer Sci.* **113**, 3826-3837.

51. Cook, A.W., and Toseland,C.P. (2021) The roles of nuclear myosin in the DNA damage response. *J. Biochem*., **69**, 265-271.

52. Fili, N., Hari-Gupta, Y., dos Santos, A., Cook, A., Poland, S., Ameer-Beg, S.M., Parsons, M. and Toseland,C.P. (2017) NDP52 activates nuclear myosin VI to enhance RNA polymerase II transcription. *Nat. Commun*., **8**, 1871.

53. Tajik, A., Zhang, Y., Wei, F., Sun, J., Jia, Q., Zhou, W., Singh, R., Khanna, N., Belmont, A.S., and Wang, N. (2016) Transcription upregulation via force-induced direct stretching of chromatin. *Nat. Mater.* **15**, 1287 –1296.

54. Dupont, S., and Wickström, S.A. (2022) Mechanical regulation of chromatin and transcription. *Nat. Rev. Genet.* **23**, 624-643.

55. Yuan, L., Roy, B., Ratna, P., Uhler, C., and Shivashankar, G.V. (2022) Lateral confined growth of cells activates Lef1 dependent pathways to regulate cell-state transitions. *Sci. Rep.* **12**, 17318.

56. Kidiyoor, G.R,. Li, Q., Bastianello, G., Bruhn, C., Giovannetti, I., Mohamood, A., Beznoussenko, G.V., Mironov, A., Raab, M., Piel, M., et al. (2020) ATR is essential for preservation of cell mechanics and nuclear integrity during interstitial migration. *Nat. Commun.* **11**, 4828.

57. Shah, P., McGuigan, C.W., Cheng, S., Vanpouille-Box, C., Demaria, S., Weiss, R.S., and Lammerding, J. (2022) ATM Modulates Nuclear Mechanics by Regulating Lamin A Levels. *Front. Cell Dev. Biol.* **10**, 875132.

58. Novikov, N.M., Zolotaryova, S.Y., Gautreau, A.M., and Denisov, E.V. (2021) Mutational drivers of cancer cell migration and invasion. *Br. J. Cancer.* **124**, 102-114.

59. Golloshi, R., Playter, C., Freeman, T.F., Das, P., Raines, T.I., Garretson, J.H., Thurston, D., and McCord, R.P. (2022) Constricted migration is associated with stable 3D genome structure differences in cancer cells. *EMBO Rep*. **23**, e52149.

60. Misteli T. (2020) The Self-Organizing Genome: Principles of Genome Architecture and Function. *Cell* **183**, 28-45.

61. Mohammed, D., Versaevel, M., Bruyère, C., Alaimo, L., Luciano, M., Vercruysse, E., Procès, A., and Gabriele, S. (2019) Innovative Tools for Mechanobiology: Unraveling Outside-In and Inside-Out Mechanotransduction. *Front. Bioeng. Biotechnol.* **7**, 162.

62. Finan, J.D., Chalut, K.J., Wax, A., Guilak, F. (2009) Nonlinear osmotic properties of the cell nucleus. *Ann Biomed Eng.* **37**, 477-91.

63. Funkhouser, C.M., Sknepnek, R., Shimi, T., Goldman, A.E., Goldman, R.D., Olvera de la Cruz, M. (2013) Mechanical model of blebbing in nuclear lamin meshworks. *Proc. Natl. Acad. Sci. USA* 110, 3248-53.

64. Nawaz, S., Sánchez, P., Bodensiek, K., Li, S., Simons, M., and Schaap, I.A. (2012) Cell visco-elasticity measured with AFM and optical trapping at sub-micrometer deformations. *PLoS One.* **7**, e45297.

65. Daza, R., González-Bermúdez, B., Cruces, J., De la Fuente, M., Plaza, G.R., Arroyo-Hernández, M., Elices, M., Pérez-Rigueiro, J., and Guinea, G.V. (2019) Comparison of cell mechanical measurements provided by Atomic Force Microscopy (AFM) and Micropipette Aspiration (MPA). *J. Mech. Behav. Biomed. Mater.* **95**, 103-115.

64. Madrazo, E., González-Novo, R., Ortiz-Placín, C., García de Lacoba, M., González-Murillo, Á., Ramírez, M., and Redondo-Muñoz, J. (2022). Fast H3K9 methylation promoted by CXCL12 contributes to nuclear changes and invasiveness of T-acute lymphoblastic leukemia cells. *Oncogene* **41**, 1324-1336.

65. Hari-Gupta, Y., Fili, N., Dos Santos, Á., Cook, A.W., Gough, R.E., Reed, H.C.W., Wang, L., Aaron, J., Venit, T., Wait, E., Grosse-Berkenbusch, A., Gebhardt, J.C.M., Percipalle, P., Chew, T.L., Martin-Fernandez, M., and Toseland, C.P. (2022) Myosin VI regulates the spatial organisation of mammalian transcription initiation. *Nat Commun.* **13**, 1346.
66. dos Santos, A., Fili, N., Hari-Gupta, Y., Gough, R.E., Wang, L., Martin-Fernandez, M., Arron, J., Waite, E., Chew, T.L., and Toseland, C.P. (2022) Binding partners regulate unfolding of myosin VI to activate the molecular motor. *Biochemical J.* **479**, 1409-1428.
67. Cortazar, A.R., Torrano, V., Martín-Martín, N., Caro-Maldonado, A., Camacho, L., Hermanova, I., Guruceaga, E., Lorenzo-Martín, L.F., Caloto, R., Gomis, R.R., et al. (2018) CANCERTOOL: A Visualization and Representation Interface to Exploit Cancer Datasets. *Cancer Res.* **78**, 6320-6328.

FIGURE LEGENDS

Figure 1. Persistent 3D cell confinement promotes permanent morphological changes in the nucleus. (A) Jurkat cells (control) were embedded in a 3D collagen matrix (3.3 mg/mL) in complete medium and maintained in culture for 10 days. Then, the collagen gel was disaggregated mechanically, and transformed (TR) cells were collected, kept in suspension without any further constriction, and expanded as TR cells. **(B)** Control and TR cells were sedimented on poly-L-lysine coated coverslips, fixed, and stained with Hoechst for their analysis by confocal microscopy. Right panels indicate the shape of the nuclei in black. Bar 10 µm. **(C)** Graph shows changes in the nuclear area of control and TR cells. Mean n=522 cells ± SD (3 independent replicates). **(D)** Graph shows changes in the nuclear circularity of control and TR cells. Mean n=545 cells ± SD (3 independent replicates). **(E)** Nuclei from control (blue) and TR (red) cells were isolated and their complexity (SSC-A) and size (FSC-A) determined by flow cytometry. Right panel indicates the geometric mean of both characteristics for both populations. **(F)** Control and TR cells were collected and processed for thin section electron microscopy to visualize the nuclear morphology. Right panels indicate the shape of the nuclei in black. *** $P<0.001$.

Figure 2. Persistent 3D cell confinement induces PKC-dependent redistribution of lamin B1 in TR cells. (A) Control or TR cells were seeded on poly-L-lysine-coated glasses and stained with Hoechst (blue) and anti-lamin B1 antibody (red) for their analysis by confocal microscopy. Bar 10 µm. **(B)** Line plots show the signal profile of lamin B1 for longitudinal sections from 15 representative cells from (A). Red line indicates the mean intensity of the profiles analyzed. **(C)** Representative middle cross-section planes of control and TR cells stained as in (A). White arrows in ortogonal views indicate lamin B1 invaginations. **(D)** TR cells were transfected with siRNA control or against PKCβ for 24 h. Then, cells were seeded on poly-L-lysine-coated glasses and stained with Hoechst (blue) and anti-lamin B1 antibody (red) for their analysis by confocal microscopy. Bar 10 µm. **(E)** Line plots show the signal profile of lamin B1 for longitudinal sections from 15 representative cells from 15 representative cells from (D). Red line indicates the mean intensity of the profiles analyzed.

Figure 3. Actin polymerization modulates the aberrant distribution of lamin B1 in TR cells. (A) TR cells were treated or not with 2µg/mL latrunculin B (an inhibitor of actin polymerization) or 1µg/mL jasplakinolide (an actin polymerization stabilizer) for 1 h. Then, cells were seeded on poly-L-lysine-coated glasses and stained with Hoechst (blue) and anti-lamin B1 antibody (red) for their analysis by confocal microscopy. Bar 10 µm. **(B)** Line plots show the signal profile of lamin B1 from 15 representative cells from (A). Red line indicates the mean intensity of the profiles analyzed. **(C)**

TR cells were transfected with different NLS-actin mutants for 48 h: NLS-YFP-WT (wild type actin), NLS-YFP-R62D (R actin to impair actin polymerization) and NLS-YFP-S14C (S actin to favour actin polymerization). Cells were seeded on poly-L-lysine-coated glasses and stained with Hoechst and anti-lamin B1 antibody (red) for their analysis by high content microscopy. Bar 10 µm. **(D)** Line plots show the signal profile of lamin B1 from 15 representative cells from (C). Red line indicates the mean intensity of the profiles analyzed. **(E)** TR cells were subjected to PKCβ silencing for 24 h or inhibition with 2 nM enzastaurin for 30 min, prior to treatment with 1µg/mL jasplakinolide for an additional hour. Then, cells were seeded on poly-L-lysine-coated glasses and stained with Hoechst and anti-lamin B1. Bar 10 µm. **(F)** Line plots show the signal profile of lamin B1 from 15 representative cells from (D). Red line indicates the mean intensity of the profiles analyzed.

Figure 4. TR cells from 3D confinement alter their transcriptional program. (A) Control or TR cells were lysed, mRNA was isolated, and transcriptional changes were analyzed by mRNA expression microarray. Volcano plot shows significant downregulated (blue) and upregulated (red) transcripts in TR cells compared to control conditions. |Fold Change| > 1.4 and P-value <0.05 (n=2 replicates). (B) Heat map shows the relative gene expression patterns of transcriptomics datasets performed in (A). **(C)** Bioinformatics analysis of gene expression changes performed with Cancertool to identify down and upregulated pathways in TR cells. **(D)** Jurkat cells were cultured in suspension (control) or embedded in a 3D collagen type I matrix for 3 hours (3D). Cells were collected, lysed, and RNA was extracted for the analysis of transcriptional changes by microarray. Volcano plot shows significant downregulated (blue) and upregulated (red) transcripts in both conditions. |Fold Change| > 1.4 and P-value <0.05 (n=3 replicates). **(E)** Venn diagram representation of common transcriptional changes between short- and long-term 3D confinement conditions. **(F)** GO/KEGG enrichment analysis of common transcriptional changes from (E).

Figure 5. TR cells from persistent 3D confinement show alterations in their cell cycle and survival response. (A) Control or TR (dark and dashed lines, respectively) cells were cultured and their cell proliferation was quantified by MTT assay at indicated times. Mean n = 5 replicates ± SD. **(B)** Control and TR cells were incubated with 5-bromo-2'-deoxyuridine (BrdU) for 4 and 20 h. Then, cells were fixed and BrdU incorporation was quantified. Mean n = 3 replicates ± SD. **(C)** Control and TR cells were collected, seeded onto poly-L-lysine coated slides, fixed and stained for γH2AX (red) and Hoechst (blue). Bar 10 µm. **(D)** The number of cells containing more than 8 γH2AX foci in each field from (C) was quantified. Graph shows the percentage of control or TR cells containing more than 8 γH2AX foci per field. n=21 (3 independent replicates). **(E)** Control and TR cells were treated with 40 µM Bleomycin for 4 hours, embedded in agarose and lysed. Alkaline comet assay by electrophoresis was performed to visualize the DNA by fluorescence microscopy. **(F)** Graph shows the tail moment analysis of the comet assay in (E). Mean n=302 cells ± SD. **(G)** Control and TR cells

were cultured in the presence of the indicated drugs (1µM, Methotrexate; 5 µg/mL, Cycloheximide; 5 µg/mL, Blasticidin S; or 10 µg/mL, Chlorambucil) for 24 h. Then, cells were collected and stained for annexin V-FITC and propidium iodide for flow cytometry analysis. Graph shows the survival ratio of control and TR cells upon normalization to their untreated conditions. Mean n = 3 replicates ± SD. *** P<0.001.

Figure 6. Aberrant cells after suffering 3D confinement exhibit reduced cell invasiveness. (A) Control and TR cells were seeded on the top chamber of Transwell inserts and allowed to migrate through 5 µm pores towards FBS for 24 h. Graphs show the percentage of migrated cells. Mean n = 3 replicates ± SD. **(B)** Control and TR cells were seeded on the top of a collagen 3D matrix and cultured at 37ºC for 24 h. Then, cells were fixed, stained with propidium iodide, and serial confocal images of the matrix were taken to calculate the depth invasion of ALL cells towards FBS. **(C)** Graph shows the percentage of cells invading into the collagen gel deeper than 100 µm. Mean n = 6 replicates ± SD. **(D)** Control (Far Red+) and TR (CFSE+) cells were stained with vital dyes, mixed 1:1 and injected into the tail vein of NSG (NOD scid gamma mouse) mice. After 24 h, labelled cells in spleen, bone marrow and liver were determined by flow cytometry. Graph shows the correlation between the control and the TR cells infiltrated into the tissues for each mouse. Mean n=14. * P<0.05. *** P<0.001.

Figure 7. Persistent 3D confinement modulates nuclear biophysics and homogeneity. (A) Isolated nuclei from control and TR cells were seeded on poly-L-lysine coated slides, stained with Hoechst, and confined mechanically up to 3 µm. Confocal images pre- and post- confinement are shown. Bar 10 µm. **(B)** Graph shows the quantification of nuclear area pre- and post-confinement from (A). **(C)** Control and TR cells were collected, and their DNA was digested with DNAse I for 8 or 15 min. Then chromatin degradation was resolved in an agarose gel. **(D)** Graph shows the DNA fragmentation profile from control (black) and TR cells (red) as in (D). Arrows indicate the maximum peak of signal in both populations. **(E)** Isolated nuclei from control and TR cells were sedimented on poly-L-lysine coated slides and DNA was stained with SiR-DNA (Spirochrome) for 1 h. Then, high resolution images were taken by STORM (Stochastic Optical Reconstruction Microscopy) microscopy Bar 10 µm. Whole control and TR cells were stained with SiR-DNA (Spirochrome) for 1 h and viewed by SIM (Structured Illumination Microscopy) microscopy. Bar 10 µm. **(F)** Left panel shows the compaction analysis based on indentation assays of isolated nuclei from control and TR cells performed with optical tweezers. The compaction parameter, decays exponentially with the indentation depth, (shown here in terms of strain, being R the indenter radius). The characteristic length, defines the compaction decay. Right graph shows the values for the isolated nuclei from control and TR expressed as the ratio. **(G)** Isolated nuclei from control and TR cells were seeded on poly-L-lysine coated dishes and imaged by AFM (Atomic Force Microscopy). PeakForce Tapping

image of a representative nucleus captured with a maximum indentation force of 0.5 nN. **(H)** Graph shows the Young's modulus values for isolated nuclei from control and TR cells. Each point corresponds to the average value for a nucleus, calculated from >10000 independent force curves. Mean n=9-13 ± SD. **P< 0.01, *** P<0.001.

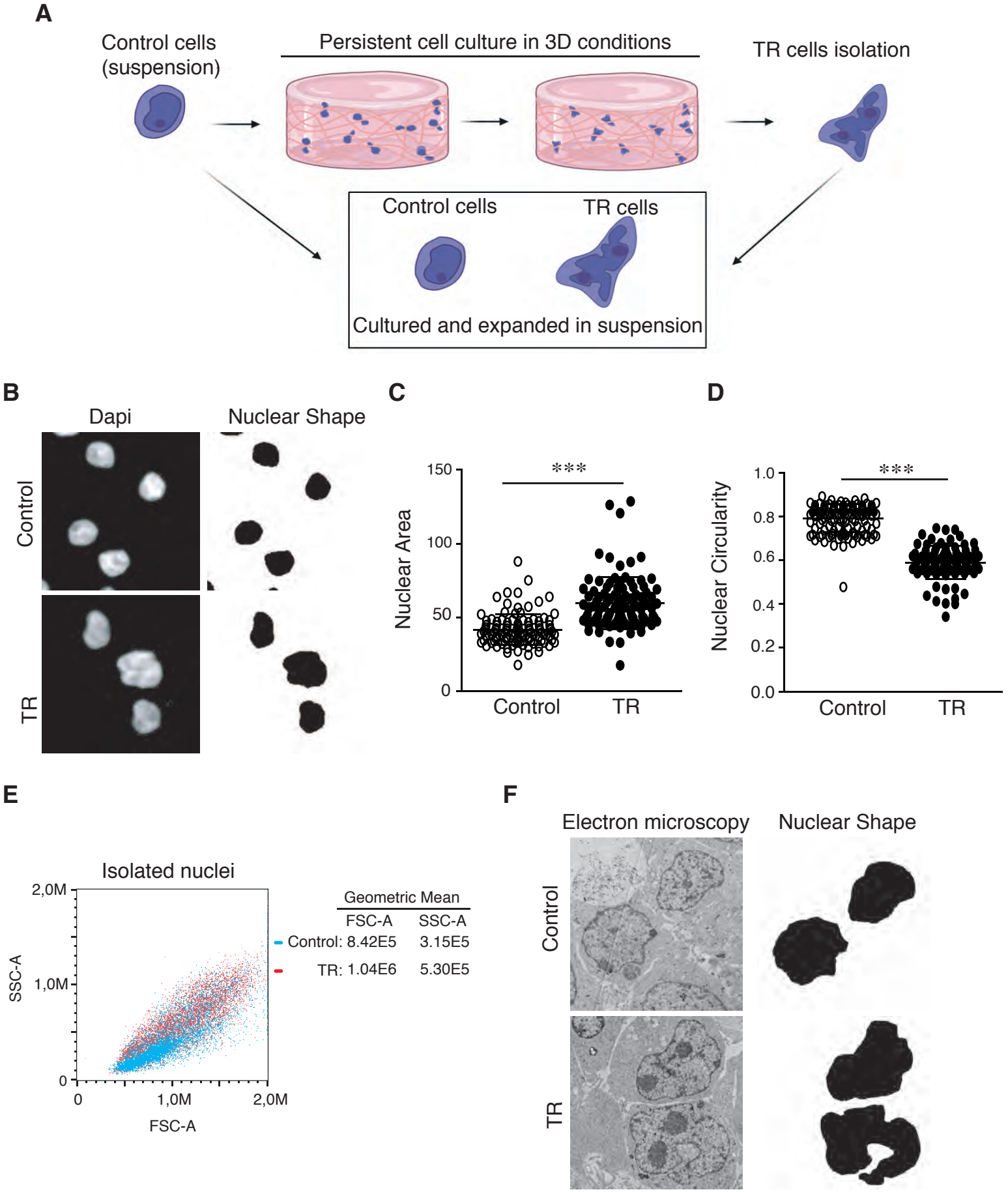
A
Control cells
(suspension)
Persistent cell culture in 3D conditions
TR cells isolation
Control cells
TR cells
Cultured and expanded in suspension
B
Dapi
Nuclear Shape
Control
TR
C
Nuclear Area
150
100
50
0
***
Control
TR
D
Nuclear Circularity
1.0
0.8
0.6
0.4
0.2
0.0
***
Control
TR
E
Isolated nuclei
SSC-A
2,0M
1,0M
0
0
1,0M
2,0M
FSC-A
Geometric Mean
FSC-A SSC-A
Control: 8.42E5 3.15E5
TR: 1.04E6 5.30E5
F
Electron microscopy
Nuclear Shape
Control
TR

Figure 1

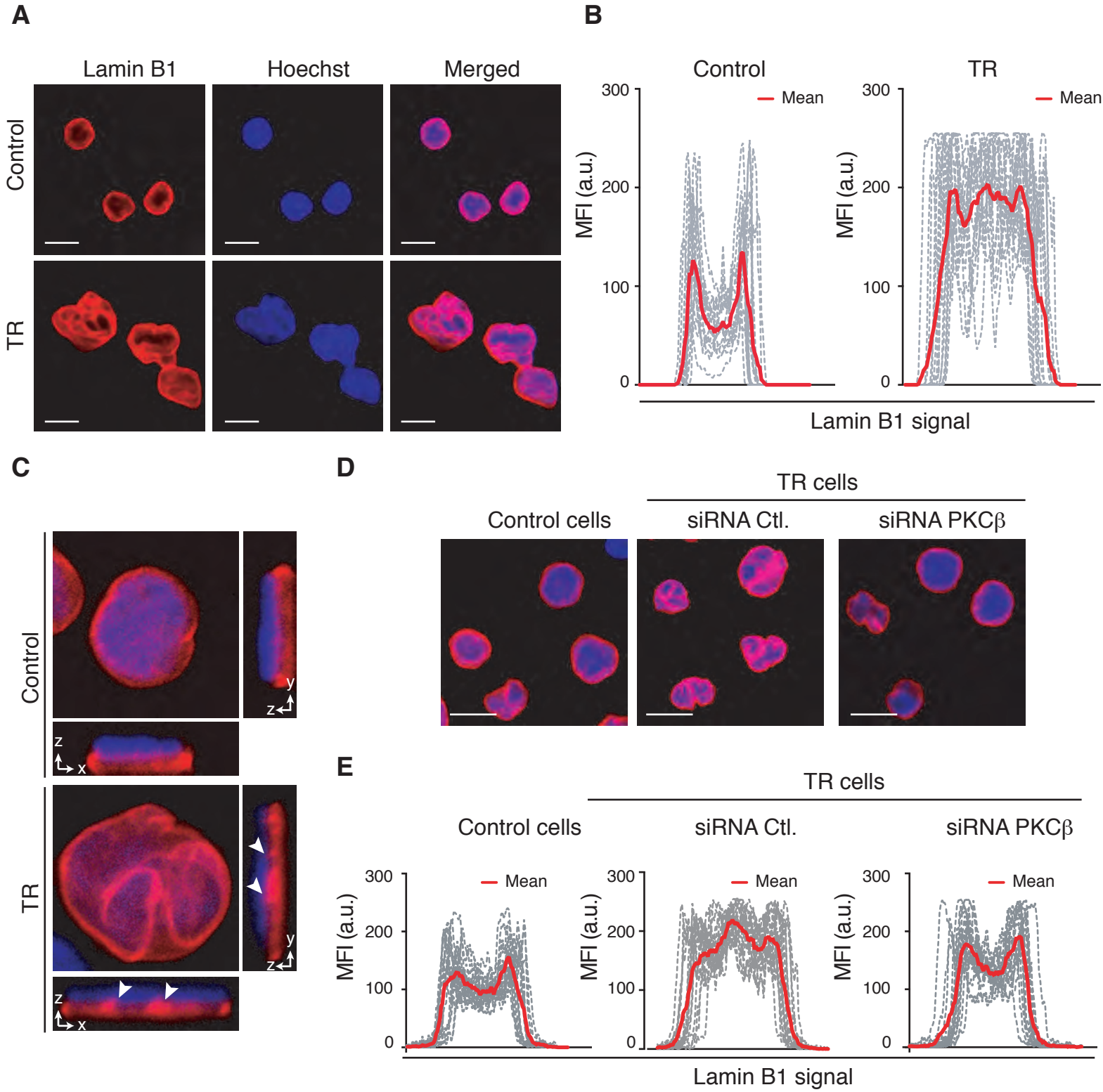
A
Lamin B1
Hoechst
Merged
Control
TR
B
Control
TR
Mean
MFI (a.u.)
300
200
100
0
Lamin B1 signal
C
Control
TR
y
z
x
D
TR cells
Control cells
siRNA Ctl.
siRNA PKCβ
E
TR cells
Control cells
siRNA Ctl.
siRNA PKCβ
Mean
MFI (a.u.)
300
200
100
0
Lamin B1 signal

Figure 2

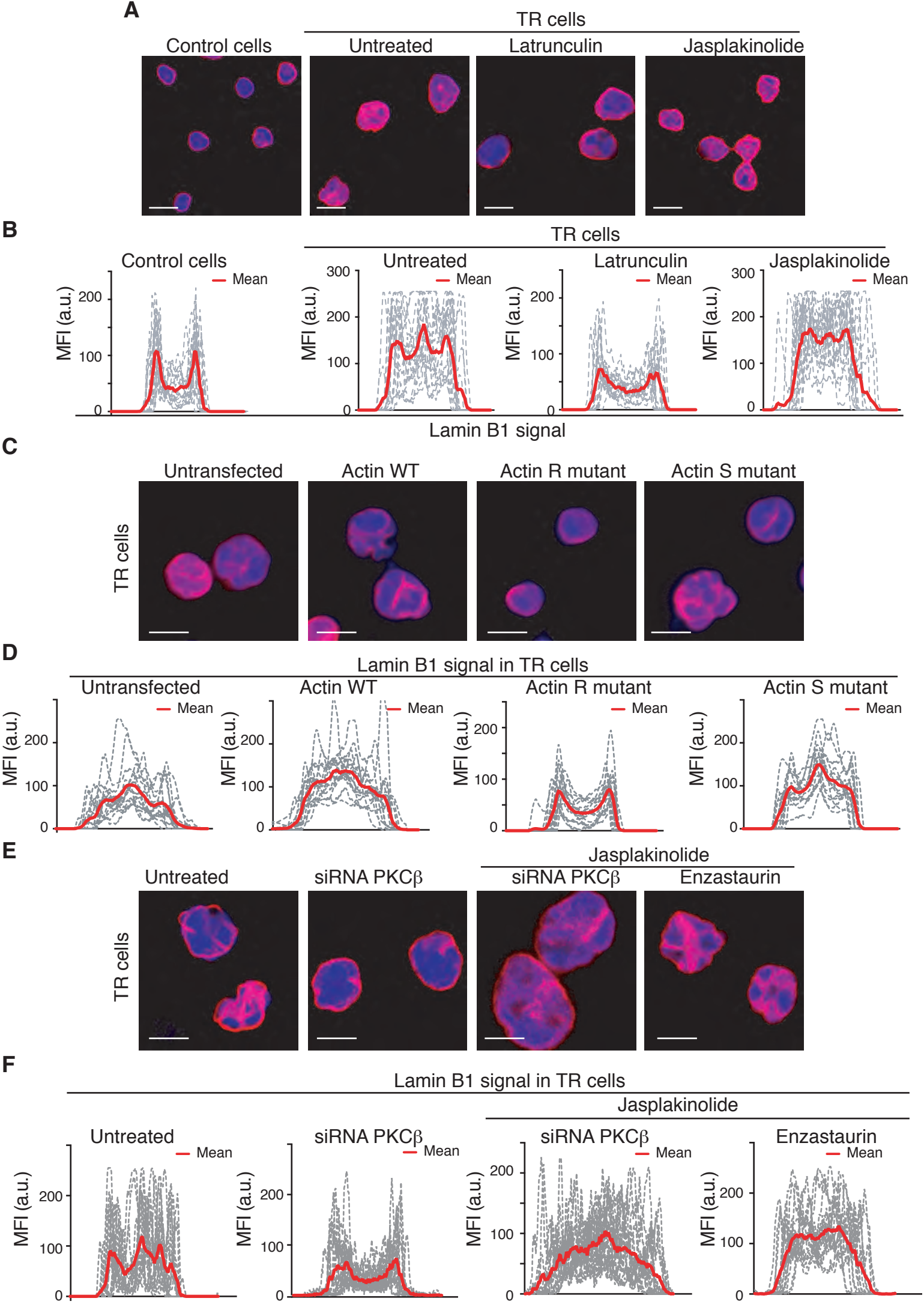
A
TR cells
Control cells
Untreated
Latrunculin
Jasplakinolide
B
TR cells
Control cells
Untreated
Latrunculin
Jasplakinolide
Mean
MFI (a.u.)
0
100
200
300
Lamin B1 signal
C
Untransfected
Actin WT
Actin R mutant
Actin S mutant
TR cells
D
Lamin B1 signal in TR cells
Untransfected
Actin WT
Actin R mutant
Actin S mutant
Mean
MFI (a.u.)
E
Jasplakinolide
Untreated
siRNA PKCβ
siRNA PKCβ
Enzastaurin
TR cells
F
Lamin B1 signal in TR cells
Jasplakinolide
Untreated
siRNA PKCβ
siRNA PKCβ
Enzastaurin
Mean
MFI (a.u.)

Figure 3

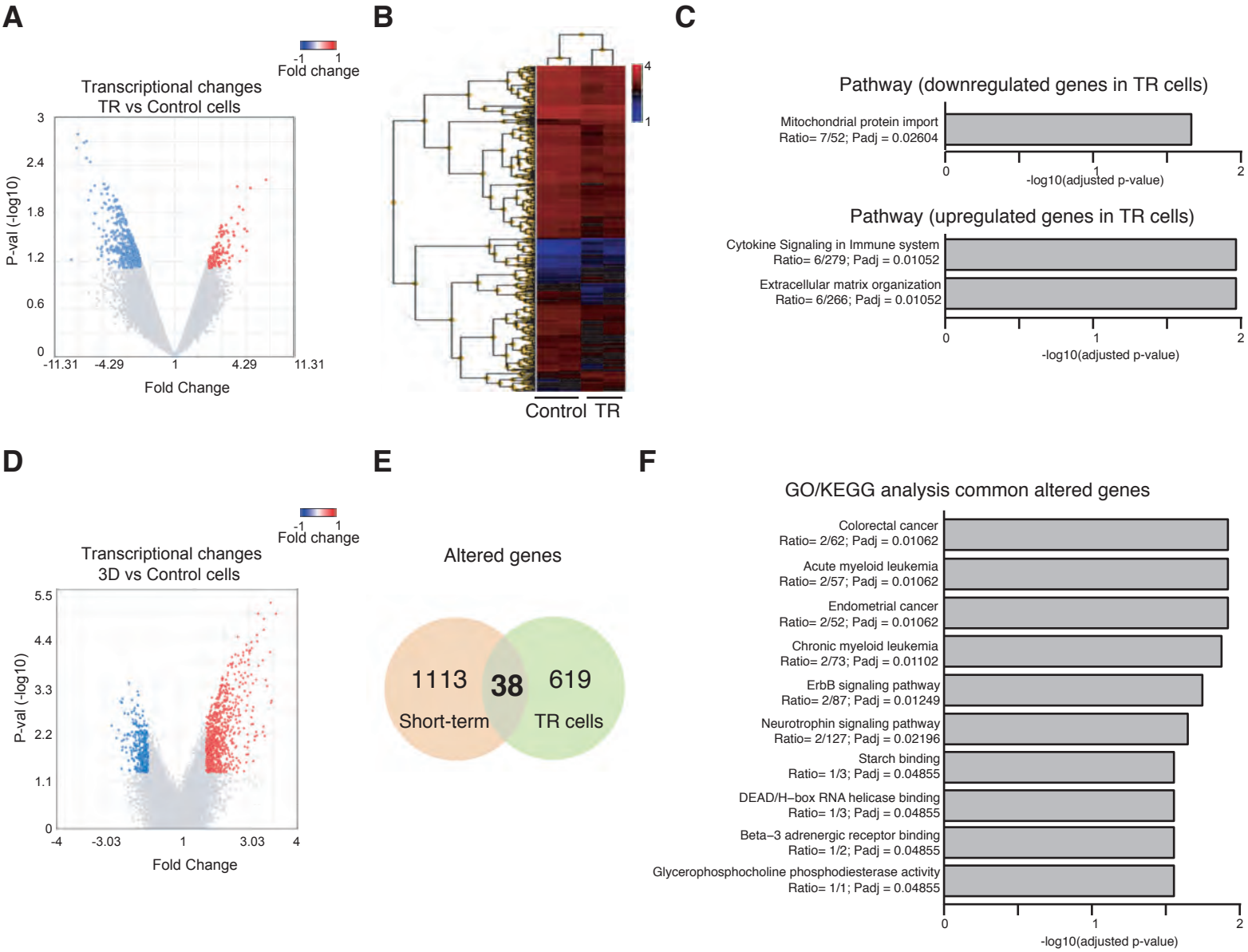
A
Fold change
-1
1
Transcriptional changes
TR vs Control cells
P-val (-log10)
3
2.4
1.8
1.2
0.6
0
-11.31
-4.29
1
4.29
11.31
Fold Change
B
4
1
Control
TR
C
Pathway (downregulated genes in TR cells)
Mitochondrial protein import
Ratio= 7/52; Padj = 0.02604
0
1
2
-log10(adjusted p-value)
Pathway (upregulated genes in TR cells)
Cytokine Signaling in Immune system
Ratio= 6/279; Padj = 0.01052
Extracellular matrix organization
Ratio= 6/266; Padj = 0.01052
0
1
2
-log10(adjusted p-value)
D
Fold change
-1
1
Transcriptional changes
3D vs Control cells
P-val (-log10)
5.5
4.4
3.3
2.2
1.1
0
-4
-3.03
1
3.03
4
Fold Change
E
Altered genes
1113
38
619
Short-term
TR cells
F
GO/KEGG analysis common altered genes
Colorectal cancer
Ratio= 2/62; Padj = 0.01062
Acute myeloid leukemia
Ratio= 2/57; Padj = 0.01062
Endometrial cancer
Ratio= 2/52; Padj = 0.01062
Chronic myeloid leukemia
Ratio= 2/73; Padj = 0.01102
ErbB signaling pathway
Ratio= 2/87; Padj = 0.01249
Neurotrophin signaling pathway
Ratio= 2/127; Padj = 0.02196
Starch binding
Ratio= 1/3; Padj = 0.04855
DEAD/H–box RNA helicase binding
Ratio= 1/3; Padj = 0.04855
Beta–3 adrenergic receptor binding
Ratio= 1/2; Padj = 0.04855
Glycerophosphocholine phosphodiesterase activity
Ratio= 1/1; Padj = 0.04855
0
1
2
-log10(adjusted p-value)

Figure 4

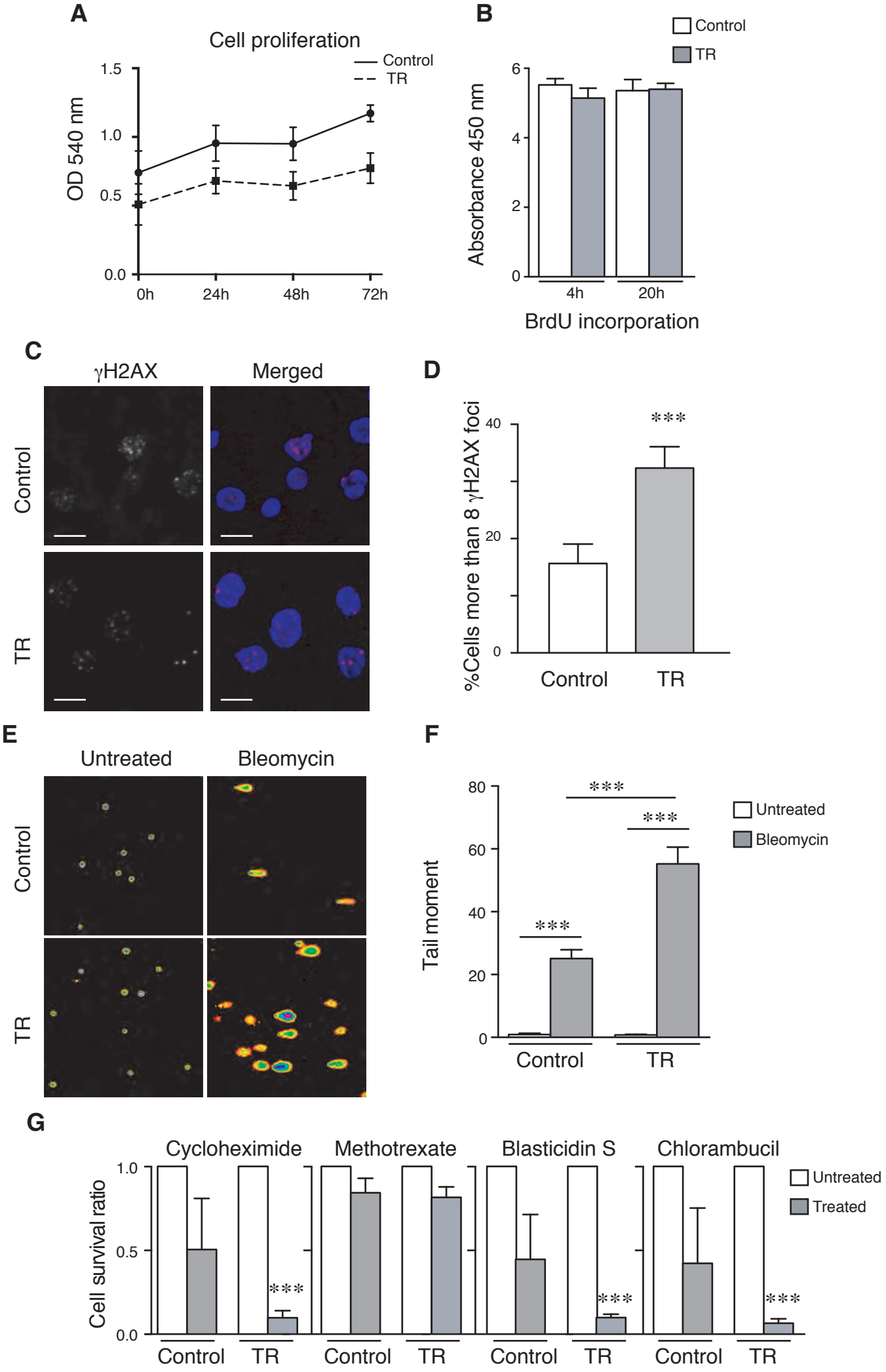
A
Cell proliferation
Control
TR
OD 540 nm
1.5
1.0
0.5
0.0
0h
24h
48h
72h
B
Control
TR
Absorbance 450 nm
6
4
2
0
4h
20h
BrdU incorporation
C
γH2AX
Merged
Control
TR
D
%Cells more than 8 γH2AX foci
40
20
0
***
Control
TR
E
Untreated
Bleomycin
Control
TR
F
Tail moment
80
60
40
20
0
***
***
***
Untreated
Bleomycin
Control
TR
G
Cycloheximide
Methotrexate
Blasticidin S
Chlorambucil
Cell survival ratio
1.0
0.5
0.0
***
***
***
Untreated
Treated
Control
TR
Control
TR
Control
TR
Control
TR

Figure 5

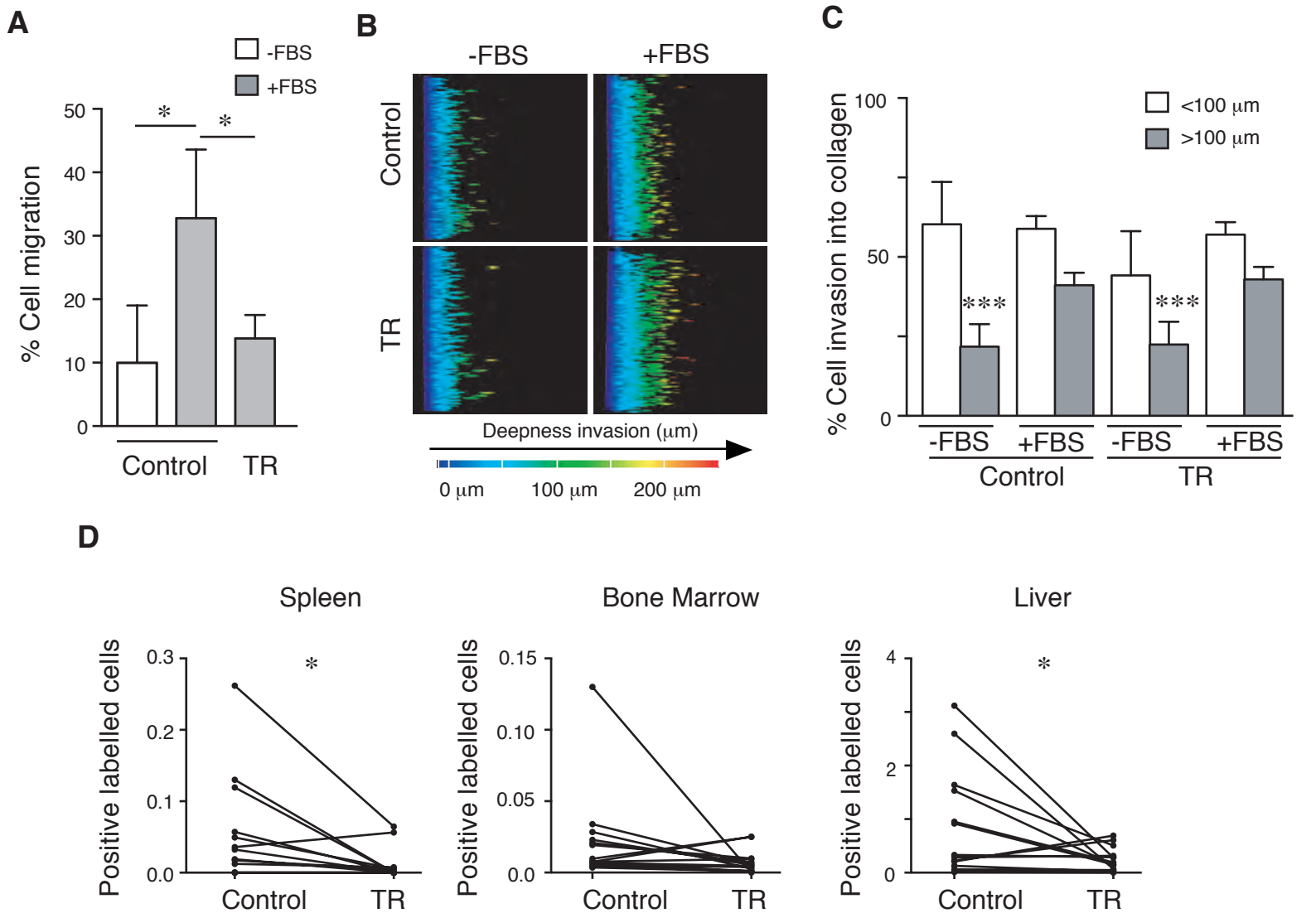
A
-FBS
+FBS
% Cell migration
50
40
30
20
10
0
*
*
Control
TR
B
-FBS
+FBS
Control
TR
Deepness invasion (μm)
0 μm
100 μm
200 μm
C
% Cell invasion into collagen
100
50
0
<100 μm
>100 μm
***
***
-FBS
+FBS
-FBS
+FBS
Control
TR
D
Spleen
Bone Marrow
Liver
Positive labelled cells
0.3
0.2
0.1
0.0
*
Control
TR
0.15
0.10
0.05
0.0
Control
TR
4
2
0
*
Control
TR

Figure 6

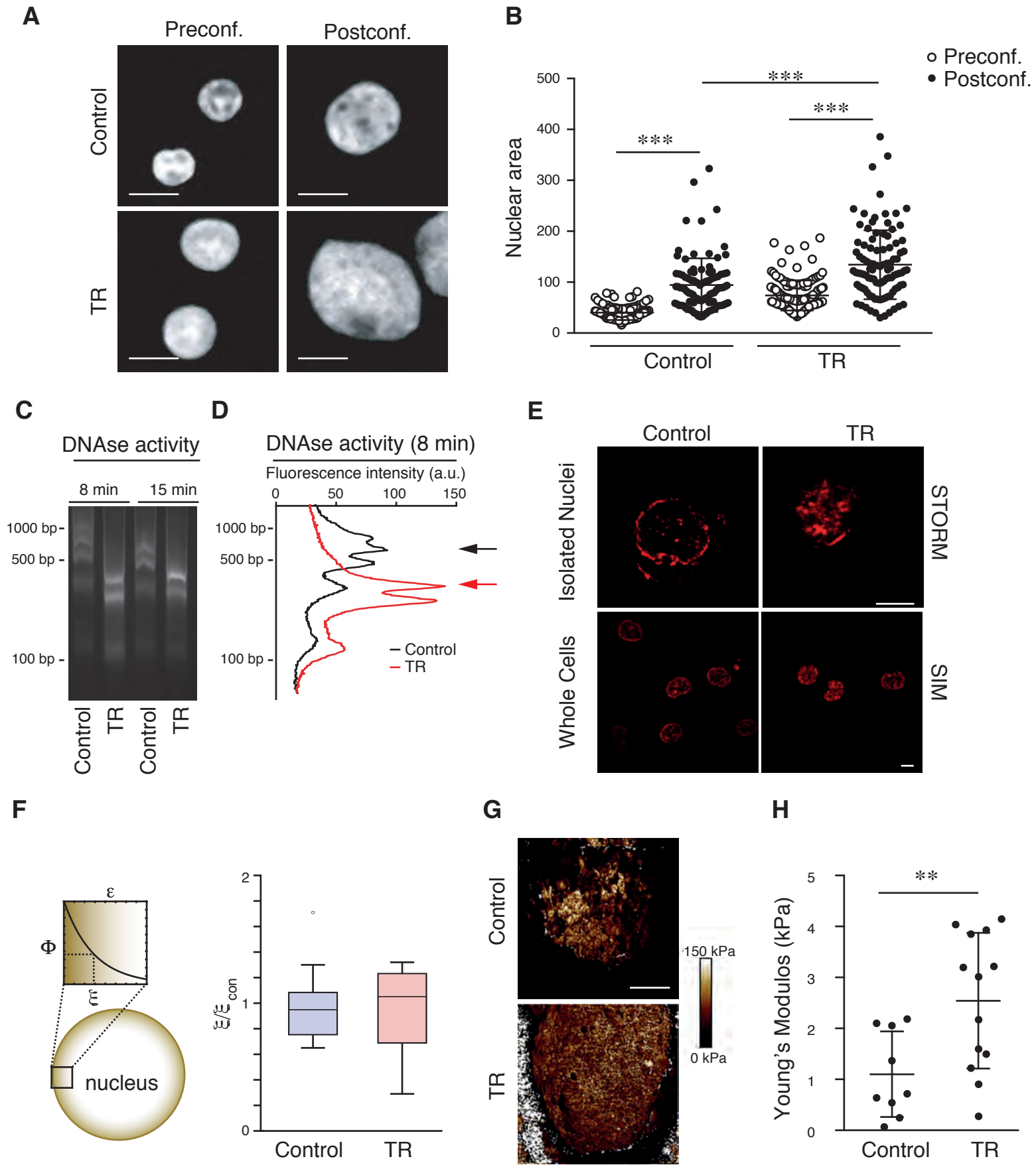
A
Preconf.
Postconf.
Control
TR
B
Preconf.
Postconf.
Nuclear area
500
400
300
200
100
0
***
***
Control
TR
C
DNAse activity
8 min
15 min
1000 bp
500 bp
100 bp
Control
TR
Control
TR
D
DNAse activity (8 min)
Fluorescence intensity (a.u.)
0
50
100
150
1000 bp
500 bp
100 bp
Control
TR
E
Control
TR
Isolated Nuclei
Whole Cells
STORM
SIM
F
ε
Φ
ξ
nucleus
ξ/ξ con
2
1
0
Control
TR
G
Control
TR
150 kPa
0 kPa
H
Young's Modulos (kPa)
5
4
3
2
1
0
**
Control
TR

Figure 7